Geochemistry, Geophysics, Geosystems®

RESEARCH ARTICLE
10.1029/2025GC012520

Key Points:

- Vent migration within the Black Rock Desert (BRD) is not consistent with any existing models for volcanic fields along the edge of the Colorado Plateau
- Forty-six new $^{40}Ar/^{39}Ar$ ages constrain BRD volcanism from 3.7 Ma to 8 ka, which includes incremental heating data from olivine
- The asthenosphere-lithosphere-volcanic system on the edge of the Colorado Plateau is inherently complex with melts likely originating in the asthenosphere

Supporting Information:

Supporting Information may be found in the online version of this article.

Correspondence to:

B. R. Jicha,
brian.jicha@wisc.edu

Citation:

Jicha, B. R., Rivera, T. A., & Golos, E. M. (2025). Spatiotemporal evolution of volcanism in the Black Rock Desert volcanic field, Utah, and its migration relative to the Colorado Plateau. *Geochemistry, Geophysics, Geosystems*, *26*, e2025GC012520. https://doi.org/10.1029/2025GC012520

Received 18 JUN 2025
Accepted 9 SEP 2025

Author Contributions:

Conceptualization: Brian R. Jicha, Tiffany A. Rivera
Data curation: Brian R. Jicha
Formal analysis: Brian R. Jicha, Eva M. Golos
Funding acquisition: Brian R. Jicha, Tiffany A. Rivera
Investigation: Brian R. Jicha, Tiffany A. Rivera
Methodology: Brian R. Jicha, Eva M. Golos
Project administration: Brian R. Jicha

Spatiotemporal Evolution of Volcanism in the Black Rock Desert Volcanic Field, Utah, and Its Migration Relative to the Colorado Plateau

Brian R. Jicha[1], Tiffany A. Rivera[2], and Eva M. Golos[1]

[1]Department of Geoscience, University of Wisconsin-Madison, Madison, WI, USA, [2]Department of Geological Sciences, University of Missouri, Columbia, MO, USA

Abstract In the southwest USA, the Colorado Plateau is encircled by Late Cenozoic volcanic fields, most of which have eruptive histories that are marginally constrained. Establishing the spatiotemporal evolution of these volcanic fields is key for quantifying volcanic hazards and understanding magma genesis. The Black Rock Desert (BRD) volcanic field covers ~700 km^2 of west-central Utah. We present 46 new $^{40}Ar/^{39}Ar$ ages from the BRD ranging from 3.7 Ma to 8 ka, which includes $^{40}Ar/^{39}Ar$ plateau ages from olivine separates. These new ages are combined with 13 recently published $^{40}Ar/^{39}Ar$ ages from the Mineral Mountains to evaluate the spatiotemporal evolution of all five BRD subfields. The oldest lavas and domes are located to the southwest, whereas the youngest lavas, which are only a few hundred years old, are located ~30 km to the NNE. However, BRD vent migration patterns over the last 2.5 Ma are non-uniform. They are also not consistent with North American Plate motion over a partial melt zone nor have they migrated toward the center of the Colorado Plateau. BRD eruptions are almost always coincident with mapped Quaternary faults. A shear-velocity (Vs) model beneath the BRD indicates that the lithosphere has been thinned and that asthenospheric melt has coalesced at the lithosphere-asthenosphere boundary, which is supported by the trace element compositions of BRD lavas that signify that they have incorporated continental lithospheric mantle. Our data and observations suggest that the asthenosphere-lithosphere-volcanic system in the BRD is inherently complex.

Plain Language Summary Numerous volcanic fields are located along the margins of the Colorado Plateau, a major physiographic feature in the southwest U.S. Many of these volcanic fields have migrated over the timescales of millions of years. The mechanisms that control where magma is generated and where lavas erupt at the surface, along with how and why these parameters have changed through time, are unclear. We address these issues in the Black Rock Desert (BRD) in Utah using geochronologic and geochemical data from a dense array of samples to understand how the volcanic field evolved in space and time over the last 3.7 million years. We suggest that previously invoked mechanisms such as motion of the North American plate or movement toward the Colorado Plateau because of plateau ingestion are not solely responsible for controlling volcanic vent migration in the BRD. Local shallow (i.e., faults) and deep (i.e., mantle) structures seem to play an important role in where magmas are emplaced, suggesting that processes controlling magma generation, migration through the crust, and eruption are more complicated than previously envisioned.

1. Introduction

Detailed studies of volcanic fields can provide insight into lithosphere-asthenosphere interactions, timescales of magmatic processes, potential hazards, and the evolution of the field over time. The eruptive histories of distributed monogenetic basaltic volcanic fields tend to be not as extensively studied as those of stratovolcanoes or silicic caldera-forming systems because they often pose significantly less hazards than their more explosive counterparts due to their markedly lower eruptive volumes. However, numerous volcanic fields have recently been studied in unprecedented detail using geochemical, geochronologic, geomorphologic, and spatial distribution data, and have revealed important new details regarding vent morphology, vent migration and recurrence intervals (e.g., Aguilera et al., 2022; Gómez-Vasconcelos et al., 2020; Leonard et al., 2017; Zimmerer, 2024).

Several Quaternary monogenetic volcanic fields exist along a NE-SW trend at the confluence of the easternmost edge of the Basin and Range province and the western margin of the Colorado Plateau. The Black Rock Desert (BRD) volcanic field in central Utah has been the focus of numerous geochemical- and geochronologic-based studies over the last 50 years because it is the site of Utah's youngest volcanism with a moderate threat

Supervision: Tiffany A. Rivera
Writing – original draft: Brian R. Jicha
Writing – review & editing: Tiffany A. Rivera, Eva M. Golos

ranking (Ewert et al., 2018), the highest among all the volcanic fields in Colorado, Arizona, Utah, Nevada, and New Mexico. In addition, the BRD has been targeted by the U.S. Department of Energy (DOE) as a potential geothermal resource area. The DOE Frontier Observatory for Research in Geothermal Energy (FORGE) site is currently located ∼6 km west of the Bailey Ridge rhyolite flow in the Mineral Mountains of the Cove Fort subfield (Rivera et al., 2024). The BRD lava compositions are generally bimodal with abundant basalts and basaltic andesites and several rhyolites. In fact, the BRD is somewhat unique amongst all of the active volcanic fields in the SW USA in that it has erupted ∼30 km^3 of rhyolite (e.g., Rivera et al., 2024). Dozens of K-Ar and a few $^{40}Ar/^{39}Ar$ ages have been published for BRD lavas and tephras (Best et al., 1980; Crecraft et al., 1981; Evans et al., 1980; Hoover, 1974; Johnsen et al., 2010, 2014; Nash, 1986; Oviatt, 1991). Generally, these data suggest that the BRD is at least 2.7 Ma with eruptions continuing into the Holocene (Judge et al., 2019; Valastro et al., 1972). However, because the ages are imprecise and the erupted volcanics are often isolated lavas or domes, the relative stratigraphy remains a matter of debate. In the interior west of North America, bimodal volcanism typically occurs with the eruption of silicic lavas followed by basaltic lavas (e.g., Armstrong et al., 1969; Christiansen & Lipman, 1972). In the BRD, the debate centers on whether the rhyolites preceded multiple episodes of basaltic volcanism, as suggested by Crecraft et al. (1981), or whether basalts and rhyolites erupted simultaneously (e.g., Johnsen et al., 2014).

The most common approaches to understanding the magmatic processes from monogenetic volcanic fields in this region are to evaluate lava geochemistry, model geophysical data, or pair geochemistry with the geochronology. Here we build upon the wealth of existing data and observations in the BRD and present new high-precision $^{40}Ar/^{39}Ar$ ages, which are used to refine the eruptive chronostratigraphy and constrain the rates and patterns of vent migration. However, what distinguishes this study from the numerous others is that we couple the geochronologic data with new and existing geochemical data, structural mapping, and a model of the local shear velocity structures to attempt to understand where BRD magmas are generated (lithosphere versus asthenosphere) and elucidate the role of tectonics in determining where eruptions occur within a distributed volcanic field.

2. Geologic Setting

The BRD volcanic field is located within the Sevier Desert of central Utah near the boundary between the Colorado Plateau and the Basin and Range physiographic provinces. It is bound by the Cricket Mountains to the west, which primarily consist of Cambrian quartzites and limestones. To the east lie exposed rocks with a variety of lithologies and ages, including Precambrian and Cambrian quartzites, Mississippian to Cretaceous limestones, sandstones, and conglomerates, and Pliocene to Pleistocene alluvial and gravel deposits. Nash (1986) subdivided the BRD volcanic field into five subfields from north to south: Fumarole Butte, Ice Springs, Beaver Ridge, Twin Peaks, and Cove Fort (Figure 1). The Cove Fort subfield includes the high-silica rhyolite obsidian flows and a series of coalescing porphyritic domes of the Mineral Mountains (Rivera et al., 2024 and references therein; Figure 1). The Twin Peaks subfield consists of rhyolitic composite domes (South Twin, North Twin, mid-dome) and torta-like rhyodacite domes (Coyote Hills) as well as numerous basaltic to andesitic lavas from the Cove Creek and Burnt Mountain units (Johnsen et al., 2014). The Beaver Ridge subfield is dominated by basaltic lavas with small volumes of dacite and rhyolite (White Mountain dome). The Fumarole Butte subfield is made up of isolated outcrops of basaltic andesitic lava (i.e., Fumarole Butte and south Smelter Knolls maar crater) and the rhyolitic Smelter Knolls tuff. The Ice Springs subfield is the youngest of the BRD subfields with eruptions of mafic lavas that represent the youngest volcanism in the state of Utah (Judge et al., 2019).

Numerous BRD lavas have been modified by Lake Bonneville, which filled the Sevier Basin and most of NW Utah beginning around 30 ka until it flooded into the Snake River in Idaho at 18 ka (Oviatt, 2015). The lavas from small monogenetic eruptions such as those at Sunstone Knoll and Pot Mountain have been truncated by Bonneville erosion, resulting in a flat-topped, mesa-like appearance. Shoreline terraces have been cut into the 1.1 Ma Fumarole Butte, and several of the Burnt Mountain units in the central part of the volcanic field are mantled with lacustrine limestone clasts, which occur as white boulders/cobbles that contrast with the adjacent black lavas (Galyardt & Rush, 1981).

Lake Bonneville shoreline deposits in the Sevier Desert and numerous BRD lavas have been displaced by N-S oriented surface-rupturing faults. The source of the faulting remains controversial, with some suggesting that local extension is driven by slip along the southern Wasatch Fault Zone or underlying Sevier Desert detachment

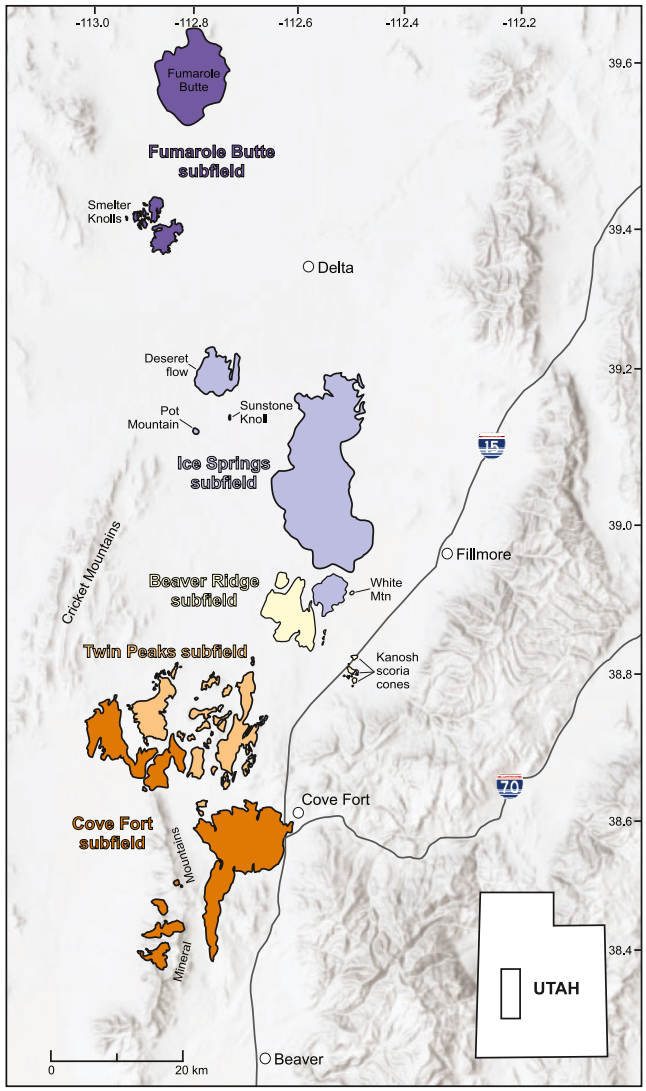

Figure 1. Map of the Black Rock Desert volcanic field in west-central Utah showing its five subfields. Base terrain map and subfield boundaries modified from Hintze et al. (2000).

(von Tish et al., 1985), whereas others suggest that extension is the result of magma-assisted rifting associated with BRD volcanism (Stahl & Niemi, 2017).

Geophysical studies have inferred a thin lithosphere below the Basin and Range, and a step-like increase in lithospheric thickness into the rigid Colorado Plateau to the east (Byrnes et al., 2023; Golos et al., 2024; Hopper & Fischer, 2018; Liu et al., 2011; Shen et al., 2013). Heat flow is also greater below the Basin and Range, with elevated values locally below the BRD (Blackwell et al., 2011). Geodynamic modeling suggests that edge-driven convection (King & Anderson, 1998) may occur within the sub-lithospheric mantle, in which upwelling occurs below the thinner Basin and Range, and downwelling below the Colorado Plateau mantle (Ballmer et al., 2015; van Wijk et al., 2010). Such a mantle flow regime may be consistent with sub-lithospheric melting, as argued by geophysical and geochemical forms of modeling (e.g., Byrnes et al., 2023; Plank & Forsyth, 2016; Rudzitis et al., 2016). Therefore, the larger-scale geodynamic context in which the BRD is found is important for evaluating magma genesis.

3. Methods

3.1. Sample Collection

Lava and tephra samples were obtained from the BRD volcanic field during multiple campaigns annually spanning 2018 to 2022. Samples were taken from the dense interior of lava flows with an emphasis on avoiding vesicle-rich or altered portions of the lava (Figure 2). Sample locations are provided in the Supporting Information.

3.2. $^{40}Ar/^{39}Ar$ Methods

Samples were crushed, sieved, and ultrasonically leached in 3M HCl for 15 min and then rinsed repeatedly with deionized water. Groundmass (180–250 μm), plagioclase (250–500 μm), olivine (355–500 μm), and sanidine (500–800 μm) separates were isolated using standard magnetic and density sorting techniques. Plagioclase and sanidine were subjected to additional leaching in 10% HF for 5 minutes. All purified separates were packaged in aluminum foil and irradiated in a cadmium-lined in-core tube at the Oregon State University reactor. The 1.1864 Ma Alder Creek sanidine (Jicha et al., 2016) was used as a neutron fluence monitor for 2- to 4-hr irradiation.

$^{40}Ar/^{39}Ar$ analyses were conducted in the WiscAr Laboratory at the University of Wisconsin-Madison. For incremental heating experiments, irradiated material (20–35 mg) was placed in a 5 mm diameter well in a copper tray and heated in 12–50 steps with a 55 W CO_2 laser. The gas released during each heating step was cleaned with two SAES GP50 getters (50 W/400°C) and an ARS cryotrap (at −125°C). For single crystal fusion experiments, the CO_2 laser was operated at 17 W for 45 s. Isotopic analyses were performed using either an Isotopx NGX-600 mass spectrometer (Mixon et al., 2022) or a Noblesse 5-collector mass spectrometer (Jicha et al., 2016). The NGX-600 was operated at a trap current of 650 μA. Isotopes ^{40}Ar, ^{39}Ar, ^{38}Ar, and ^{37}Ar were measured in the H4, H2, Ax, and L2 Faradays with an integration time of 10 s, whereas ^{36}Ar was measured on a multiplier. The measurement duration was ~450 s. Noblesse measurements were done using only multipliers and lasted ~700 s. All of the $^{40}Ar/^{39}Ar$ ages are calculated using the decay constants of Min et al. (2000) and are reported with 2σ analytical uncertainties, including the J uncertainty (Supporting Information).

Figure 2. Outcrop photos from the Black Rock Desert volcanic field. (a) Massive interior of the Mid-dome rhyolite (Twin Peaks subfield). (b) Typical outcrop of Cove Creek basalt from Twin Peaks subfield. Photo taken from near the Parr locality of a 1.99 Ma Cove Creek upper unit. (c) Smelter Knolls rhyolite of the Fumarole Butte subfield, which is flow layered and exhibits honeycomb weathering. (d) South Twin rhyolite with Cove Creek andesite (Twin Peaks subfield) on its SW flank. Circles indicate locations of dated samples and $^{40}Ar/^{39}Ar$ ages are shown in Ma. (e) Platy outcrop of the 387 ka White Mountain rhyolite (Ice Springs subfield). (f) 2.08 Ma Lower Cove Creek basalt (Twin Peaks subfield; sample 20BRD-05).

3.3. Whole Rock Major and Trace Element Analyses

Major element compositions were obtained by wavelength dispersive X-ray fluorescence (WDXRF) at Hamilton Analytical Labs, USA. WDXRF determinations were made on low-dilution (1:2 sample:flux with Li-tetraborate only) doubly fused glass beads. First fused beads were re-ground to powder in an alumina ring mill for 30 s and fused again; both fusions occurred under static conditions in a 1000°C muffle furnace. The flat surface of the doubly fused bead was ground to a 15 μm finish on diamond lapping plates and sonicated in ethanol prior to

analysis. The WDXRF measurements used a Thermo Scientific ARL PERFORM'X spectrometer operating at 45 kV accelerating voltage and 45 mA current. The system was recalibrated using ∼70 certified reference standards. Drift was monitored with in-house standards AGV-1, BHVO-1, and RGM-1 with uncertainties estimated to be better than ±0.2% (1σ). ICP-MS trace element measurements at the Colorado School of Mines followed methods of Conrey et al. (2023). Samples and glass standards were ablated using a Photon Machines Analyte 193 nm G1 ablation system and analyzed using a Varian 820 ICP-MS. Drift was corrected by measuring an in-house monitor calibrated using 18 certified reference materials. For most elements, the relative uncertainty was ±3%–5%.

4. Results

4.1. $^{40}Ar/^{39}Ar$ Age Determinations

Geochronology of Quaternary volcanic units has significantly improved over the last decade due to the development of analytical instruments with more stable electronics, which translates to less noise and more stability, resulting in more precise ages (e.g., Jicha et al., 2024; Preece et al., 2018; Zimmerer, 2024). Forty-six new $^{40}Ar/^{39}Ar$ plateau ages and two single crystal total fusion weighted mean ages were obtained from BRD lavas and tephras (Table 1; Figure 3). These ages ranged from 3.711 ± 0.004 Ma to 8 ± 5 ka. All of the age spectra meet accepted plateau criteria (Schaen et al., 2021). Because no evidence of excess argon is observed in the inverse isochron regressions, we used the plateau ages to infer the time since eruption (Table 1; Figure 3). The new $^{40}Ar/^{39}Ar$ data are generally in agreement with previously published K-Ar and $^{40}Ar/^{39}Ar$ data from select units (Best et al., 1980; Crecraft et al., 1981; Evans et al., 1980; Hoover, 1974; Johnsen et al., 2010, 2014; Nash, 1986) but are more precise. Some age discrepancies between the new and published data are discussed below. The 46 new ages are herein combined with 13 $^{40}Ar/^{39}Ar$ ages from the Mineral Mountains (i.e., Cove Fort subfield) (Rivera et al., 2024) to evaluate the spatiotemporal evolution of the entire BRD volcanic field. The duration of eruptive activity within each BRD subfield is highly variable, ranging from more than 2.6 million years (Fumarole Butte) to less than 0.45 million years (Cove Fort).

4.2. Whole Rock Major and Trace Element Analyses

The compositions of BRD lava and tephra range from basaltic to high-silica rhyolitic (47.6–77.7 wt.% SiO_2 based on anhydrous composition; Figure 4; Table S1), and have both tholeiitic and calc-alkaline affinities. With the exception of a few Beaver Ridge dacites, there are very few erupted compositions between 60 and 71 wt.% SiO_2 (Figure 4). Total alkali ($Na_2O + K_2O$) contents ranged from 3.4 to 9.1 wt.% (Figure 4a). MgO ranges from >9.0 to ∼5.0 wt.% among the BRD basalts, with lavas in the Twin Peaks subfield having the highest wt.% MgO contents (Figure 4b). Most of the BRD subfields exhibit the full range of erupted compositions from basalt to rhyolite except for the Beaver Ridge lavas, which only range from basaltic to dacitic (Figure 4).

BRD basalts are light rare earth element enriched ($La/Yb_N = 4–15$) with gently dipping heavy rare earth element (HREE) patterns (Table S2). Certain high field strength element (HFSE) concentrations such as Nb and Ta show little variation with wt.% SiO_2, whereas others (Hf, Zr, Ti) are positively correlated with SiO_2 content as well as other incompatible elements like Th, Rb, and V. Ta/Th ratios of BRD mafic lavas (<60 wt.% SiO_2) generally mimic those of other lavas from the southwest USA (Farmer et al., 2020), but are more restricted from 0.7 to 0.1 (Figure 5a). Ta/Th ratios in BRD mafic lavas show no correlation with age (Figure 5b), but do show a weak correlation with wt.% SiO_2, and therefore could be a function, in part, of differentiation. Ta/Th ratios also generally increase to the east from −112.7° to −112.4° longitude or toward the Colorado Plateau (Figure 5c). Zr/Hf ratios in BRD mafic lavas show a slight decrease ($R^2 = 0.277$) over this same interval in longitude (Figure 5d).

5. Discussion

5.1. $^{40}Ar/^{39}Ar$ Dating of Olivine in Mafic Volcanic Rocks

Jicha et al. (2024) demonstrated that clinopyroxene-hosted melt inclusions can be utilized to obtain precise and accurate $^{40}Ar/^{39}Ar$ ages for Pleistocene volcanic rocks. Olivine is another mineral that is often present in mafic volcanic rocks and it commonly hosts trapped melt inclusions (e.g., Wallace et al., 2021). Olivine has not been the subject of many $^{40}Ar/^{39}Ar$ incremental heating experiments because it does not contain K and is inferred to potentially harbor inherited Ar from the mantle or lithosphere (McDougall et al., 1969).

Table 1
Summary of $^{40}Ar/^{39}Ar$ Data

Sample #	Location/unit	Rock type	Subfield	Material	Isochron		Plateau			
					$^{40}Ar/^{36}Ar_i \pm 2\sigma$	Age (Ma) $\pm 2\sigma$	N	^{39}Ar %	MSWD	Age (Ma) $\pm 2\sigma$
22BRD-50*	Smelter Knolls rhyolite	R	Fumarole Butte	sanidine			14/23		0.96	3.711 ± 0.004
21BRD-39	Coyote Hills rhyodacite	R	Twin Peaks	groundmass	301.7 ± 4.2	2.429 ± 0.026	38/38	100.0	0.79	2.448 ± 0.005
18BRDST-1	South Twin rhyolite	R	Twin Peaks	groundmass	294.3 ± 5.3	2.445 ± 0.005	18/29	64.0	1.11	2.443 ± 0.002
18BRDCM-1**	Cudahy Mine pumice	R	Twin Peaks	sanidine			12/14		0.51	2.435 ± 0.001
20BRD-09	Coyote Hills rhyodacite	R	Twin Peaks	groundmass	297.1 ± 3.6	2.423 ± 0.006	27/27	100.0	1.29	2.421 ± 0.003
20BRD-06	Mid-dome rhyolite	R	Twin Peaks	sanidine	299.5 ± 7.1	2.414 ± 0.004	23/36	75.9	0.96	2.414 ± 0.002
18BRDNT-1	North Twin rhyolite	R	Twin Peaks	sanidine	300.7 ± 4.9	2.406 ± 0.007	22/26	97.9	1.30	2.407 ± 0.003
22BRD-52	proto-Cove Creek	B	Twin Peaks	groundmass	299.4 ±1.0	2.256 ±0.063	50/50	100.0	0.83	2.296 ± 0.038
22BRD-49	Cove Creek lower	BA	Twin Peaks	groundmass	300.9 ± 3.5	2.209 ± 0.136	13/26	85.3	0.49	2.289 ± 0.058
20BRD-05	Cove Creek upper	B	Twin Peaks	groundmass	298.5 ± 1.4	2.085 ± 0.048	34/48	85.4	0.85	2.082 ± 0.023
20BRD-11	Cove Creek lower	A	Twin Peaks	groundmass	298.5 ± 2.1	2.050 ± 0.132	15/15	100.0	0.83	2.049 ± 0.064
20BRD-13	Cove Creek lower	A	Twin Peaks	groundmass	297.5 ± 2.0	2.151 ± 0.196	35/35	100.0	0.55	2.047 ± 0.061
21BRD-26	Cove Creek upper	B	Twin Peaks	groundmass	297.2 ± 2.8	2.023 ± 0.083	20/22	98.7	0.78	1.986 ± 0.029
22BRD-48	proto-Cove Creek	B	Twin Peaks	groundmass	297.9 ± 2.8	1.982 ± 0.022	17/18	99.7	0.97	1.978 ± 0.016
20BRD-12	Cove Creek lower	A	Twin Peaks	groundmass	298.3 ± 1.7	1.980 ± 0.027	16/16	100.0	0.77	1.976 ± 0.015
21BRD-29	Cove Creek lower	A	Twin Peaks	groundmass	297.4 ± 4.4	1.970 ± 0.027	25/29	96.4	0.69	1.963 ± 0.011
22BRD-46	Cove Creek upper	B	Twin Peaks	olivine	298.1 ± 1.7	1.974 ± 0.258	14/16	96.7	1.09	1.903 ± 0.118
20BRD-10	Cove Creek lower	BA	Twin Peaks	groundmass	296.9 ± 2.9	1.774 ± 0.178	21/31	81.1	1.19	1.673 ± 0.059
21BRD-27	Burnt Mountain 1 (BM1)	BA	Twin Peaks	plagioclase	299.0 ± 3.2	1.563 ± 0.076	11/17	79.8	0.77	1.572 ± 0.040
21BRD-42	Beaver Ridge I	B	Beaver Ridge	groundmass	298.0 ± 3.6	1.226 ± 0.039	15/27	78.6	0.63	1.221 ± 0.014
21BRD-33	Beaver Ridge I	D	Beaver Ridge	groundmass	299.3 ± 8.5	1.204 ± 0.110	14/20	89.2	0.12	1.213 ± 0.034
21BRD-43	Beaver Ridge I	A	Beaver Ridge	groundmass	304.9 ± 9.7	1.094 ± 0.137	20/24	94.7	0.35	1.183 ± 0.017
21BRD-37	Fumarole Butte	BA	Fumarole Butte	groundmass	295.9 ± 3.9	1.154 ± 0.090	29/32	94.5	0.48	1.096 ± 0.020
21BRD-44	Beaver Ridge I	D	Beaver Ridge	groundmass	302.8 ± 11.1	1.034 ± 0.113	10/32	57.8	0.70	1.074 ± 0.040
21BRD-41	Beaver Ridge I	B	Beaver Ridge	plagioclase	303.2 ± 13.1	1.000 ± 0.182	14/14	100.0	0.58	1.063 ± 0.039
21BRD-32	Beaver Ridge I	B	Beaver Ridge	plagioclase	299.1 ± 5.9	1.052 ± 0.102	14/14	100.0	1.08	1.060 ± 0.042
21BRD-34	Beaver Ridge I	B	Beaver Ridge	plagioclase	297.0 ± 7.8	1.035 ± 0.143	12/12	100.0	0.62	1.007 ± 0.046
20BRD-18	Beaver Ridge I	B	Beaver Ridge	plagioclase	298.1 ± 2.2	0.946 ± 0.031	22/22	100.0	0.68	0.937 ± 0.022
20BRD-19	Beaver Ridge I	B	Beaver Ridge	plagioclase	292.2 ± 20.2	0.967 ± 0.172	12/12	100.0	0.35	0.913 ± 0.043
22BRD-45	Kanosh basalt	B	Beaver Ridge	groundmass	299.8 ± 2.7	0.653 ± 0.532	33/44	92.8	0.30	0.884 ± 0.146
18BRDBR-1***	Black Rock lava	B	Cove Fort	plagioclase	298.7 ± 0.7	0.856 ± 0.039	61/65	91.5	0.91	0.865 ± 0.030
17MMBR-1***	Bailey Ridge	R	Cove Fort	glass	307.0 ± 11.0	0.848 ± 0.005	12/17	77.3	1.20	0.851 ± 0.003
21BRD-28	Burnt Mountain 2 (BM2)	BA	Twin Peaks	groundmass	298.6 ± 4.0	0.836 ± 0.064	24/28	90.7	0.86	0.837 ± 0.028
18BRDSK-1	Sunstone Knoll	B	Ice Springs	groundmass	298.5 ± 0.5	0.834 ± 0.020	18/18	100.0	0.56	0.832 ± 0.015
20BRD-03	Burnt Mountain 2 (BM2)	BA	Twin Peaks	groundmass	297.6 ± 1.5	0.871 ± 0.064	47/55	92.6	0.45	0.825 ± 0.022
18BRDPM-1	Pot Mountain	BA	Ice Springs	groundmass	298.4 ± 0.5	0.794 ± 0.027	13/17	81.1	0.63	0.788 ± 0.015
17MMWCF-1***	Wildhorse Canyon dome	R	Cove Fort	glass	300.7 ± 7.9	0.772 ± 0.055	32/33	98.2	1.07	0.786 ± 0.005
17MMWDN-1***	Wildhorse Dome North	R	Cove Fort	sanidine	298.2 ± 3.7	0.767 ± 0.006	18/19	95.1	0.33	0.766 ± 0.003
17MMWDS-1***	Wildhorse Dome South	R	Cove Fort	sanidine			8/11		0.86	0.758 ± 0.006

Table 1
Continued

Sample #	Location/unit	Rock type	Subfield	Material	Isochron		Plateau			
					$^{40}Ar/^{36}Ar_i \pm 2\sigma$	Age (Ma) ± 2σ	N	^{39}Ar %	MSWD	Age (Ma) ± 2σ
22BRD-54***	Crater Knoll	BA	Cove Fort	groundmass	299.8 ± 3.7	0.736 ± 0.053	21/36	70.9	0.63	0.754 ± 0.014
22BRD-53***	Cunningham Wash	BA	Cove Fort	groundmass	300.1 ± 3.2	0.724 ± 0.052	29/42	84.3	0.71	0.748 ± 0.014
18BRD-21	Burnt Mountain 2 (BM2)	BA	Twin Peaks	groundmass	297.8 ± 3.3	0.751 ± 0.026	14/15	98.3	1.02	0.746 ± 0.013
18BRDLR-1	Burnt Mountain 3 (BM3)	B	Twin Peaks	groundmass	301.3 ± 6.5	0.736 ± 0.015	11/15	91.6	0.60	0.742 ± 0.004
20BRD-02	Burnt Mountain 3 (BM3)	B	Twin Peaks	groundmass	297.9 ± 1.6	0.747 ± 0.018	22/27	89.1	0.79	0.741 ± 0.010
20BRD-01	Burnt Mountain 2 (BM2)	BA	Twin Peaks	groundmass	297.7 ± 3.1	0.747 ± 0.053	20/26	90.2	0.75	0.732 ± 0.014
21BRD-30	Beaver Ridge II	B	Beaver Ridge	groundmass	298.0 ± 2.4	0.705 ± 0.099	36/36	100.0	0.81	0.684 ± 0.034
18BRDDF-1	Deseret flow	B	Ice Springs	groundmass	298.8 ± 0.7	0.594 ± 0.039	10/14	96.8	0.75	0.603 ± 0.017
17MMLBM-1***	Little Bearskin Mountain	R	Cove Fort	sanidine	303.0 ± 24.0	0.578 ± 0.017	16/17	96.2	0.88	0.588 ± 0.007
17MMBM-2***	Bearskin Mountain	R	Cove Fort	sanidine	294.0 ± 10.0	0.537 ± 0.009	13/26	87.4	0.48	0.539 ± 0.004
20BRD-17	Beaver Ridge II	B	Beaver Ridge	groundmass	298.2 ± 2.7	0.536 ± 0.080	20/24	94.6	0.88	0.525 ± 0.028
20BRD-16	Beaver Ridge II	B	Beaver Ridge	groundmass	297.0 ± 3.6	0.574 ± 0.114	27/30	91.7	0.47	0.521 ± 0.026
17MMND-1***	North Dome	R	Cove Fort	sanidine	297.9 ± 2.4	0.514 ± 0.007	50/57	97.0	0.18	0.520 ± 0.004
17MMRCD-1***	Ranch Canyon Dome	R	Cove Fort	sanidine			14/20		1.53	0.501 ± 0.004
17MMST-1***	South Twin Flat Mountain	R	Cove Fort	sanidine	297.1 ± 3.2	0.479 ± 0.009	36/49	87.2	0.58	0.483 ± 0.004
21BRD-25***	Cove Fort lava	A	Cove Fort	groundmass	298.9 ± 3.6	0.409 ± 0.099	29/48	59.7	0.26	0.417 ± 0.023
20BRD-14	White Mountain rhyolite	R	Beaver Ridge	groundmass	295.7 ± 5.4	0.401 ± 0.026	14/26	72.8	0.78	0.387 ± 0.006
21BRD-36	Beaver Ridge 3	B	Beaver Ridge	groundmass	298.0 ± 2.8	0.309 ± 0.032	11/15	93.1	0.81	0.302 ± 0.015
22BRD-51	South Smelter Knolls basalt	B	Fumarole Butte	groundmass	297.9 ± 1.7	0.132 ± 0.016	22/22	100.0	0.92	0.127 ± 0.009
18BRDPL-2	Devil's Kitchen basalt	B	Ice Springs	groundmass	299.0 ± 1.2	0.005 ± 0.011	14/14	100.0	0.64	0.008 ± 0.005

Note. Ages calculated relative to 1.1864 Ma Alder Creek sanidine (Jicha et al., 2016) or 28.201 Ma Fish Canyon sanidine (Kuiper et al., 2008) using decay constants of Min et al. (2000). Atmospheric $^{40}Ar/^{36}Ar = 298.56 \pm 0.62$ (Lee et al., 2006). See Supporting Information S2 for complete data sets. N = number of plateau steps/number of total incremental heating steps, or number of dates used in weighted mean/total number of single crystal fusion dates. *B* = basalt, *BA* = basaltic andesite, *A* = andesite, *D* = dacite, *R* = rhyolite. * Data for the Smelter Knolls rhyolite were obtained via single crystal fusions. Age for this sample is a weighted mean of the 14 youngest $^{40}Ar/^{39}Ar$ dates. ** Data for the Cudahy Mine pumice were obtained via single crystal fusions. Age for this sample is a weighted mean of the 12 youngest $^{40}Ar/^{39}Ar$ dates. *** Data from Rivera et al. (2024).

Olivine was targeted in sample 22BRD-46 because the groundmass has numerous vesicles (Figure 6a), which often contain abundant trapped atmospheric Ar that can mask or overwhelm the minor amount of radiogenic Ar in the sample, thereby making it difficult to obtain an $^{40}Ar/^{39}Ar$ age determination. Olivine is an early liquidus phase in mafic magmas, and thus it can crystallize prior to magma depressurization and vesicle formation. Sample 22BRD-46 lies atop a ~70 m section of upper Cove Creek lavas (Twin Peaks subfield) (Figure 6b), the lowermost of which has been $^{40}Ar/^{39}Ar$ dated at 2.08 ± 0.02 Ma (Figure 6d). Because most of the outcrops in the BRD are isolated, low lying lavas, this section provides an opportunity to constrain the duration of mafic Cove Creek volcanism at this locality. A 16-step incremental heating experiment on olivine using the NGX-600 mass spectrometer yielded a plateau with 96.7% of the ^{39}Ar released and an age of 1.90 ± 0.12 Ma, which is consistent with the stratigraphy (Figure 6c). The 1.90 Ma age extends the duration of upper Cove Creek volcanism within the Twin Peaks subfield to ~180 kyrs (2.08–1.90 Ma). Previous estimates from Johnsen et al. (2014) suggested that Cove Creek lavas erupted from 2.2 to 2.1 Ma. Olivine from another upper Cove Creek basalt at the Parr locality gives a plateau age of 2.01 ± 0.15 Ma, which is indistinguishable from the groundmass age of 1.99 ± 0.03 Ma. The K/Ca release patterns in the two olivine experiments are very similar to those in clinopyroxene, which were clearly shown through electron imaging and K-mapping (Jicha et al., 2024) to be the result of degassing of trapped

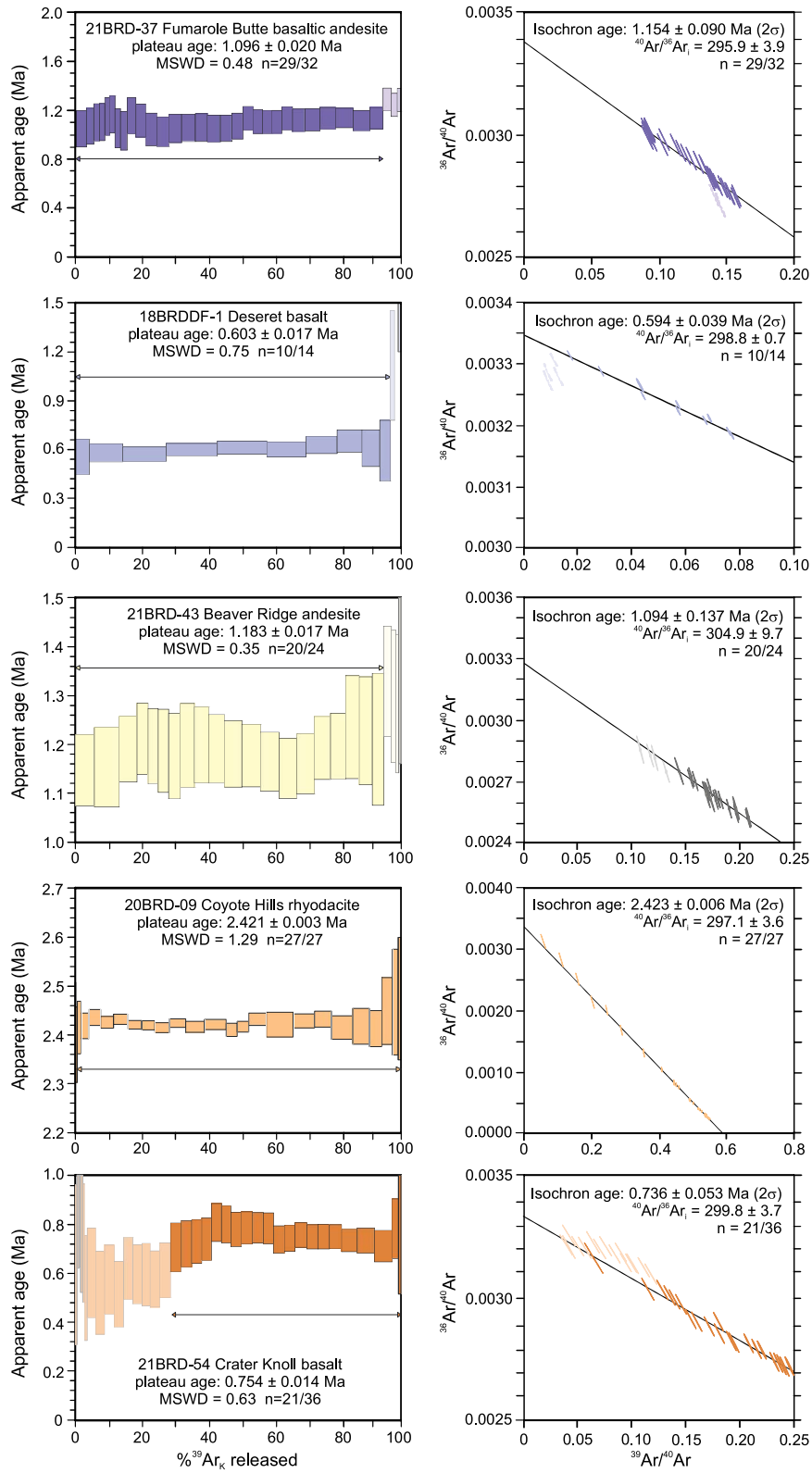

Figure 3. Representative $^{40}Ar/^{39}Ar$ age spectra and isochron diagrams for BRD samples from each subfield. Color scheme of samples matches those of the BRD subfields in Figure 1. Arrows indicate the extent of age plateau. Data from sample 21BRD-54 (Cove Fort subfield) is from Rivera et al. (2024).

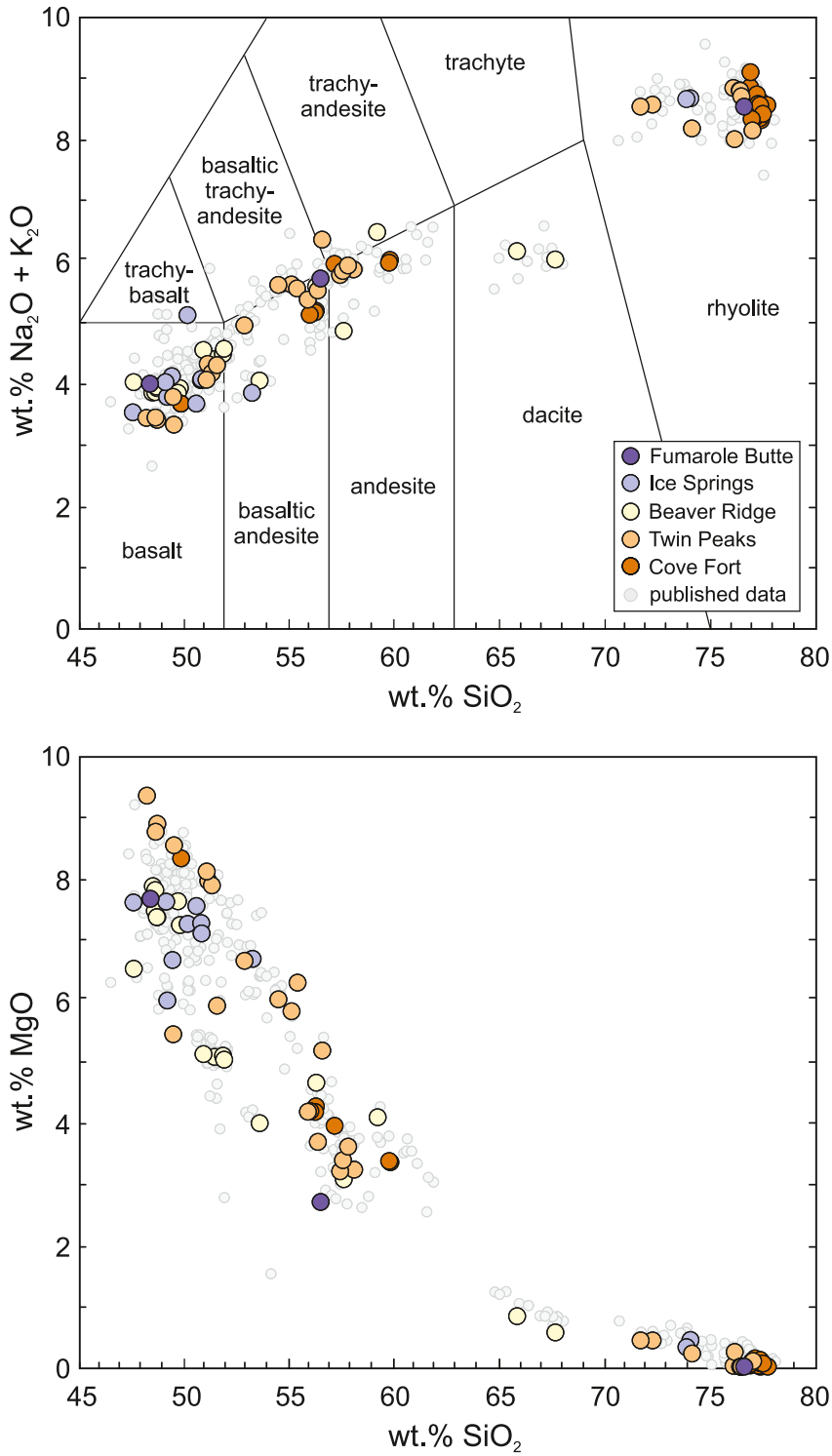

Figure 4. (a) Total Alkali versus Silica (TAS) diagram (Le Bas et al., 1986) showing the whole-rock compositions of various BRD units. (b) wt.% MgO versus wt.% SiO_2 Harker diagram. Colored circles represent data from this study and Rivera et al. (2024). Published BRD data (gray circles) from Nash (1986), Hoover (1974), Johnsen et al. (2010), Oviatt and Nash (1989), Nelson and Tingey (1997), Johnsen et al. (2014), and Oviatt (1991).

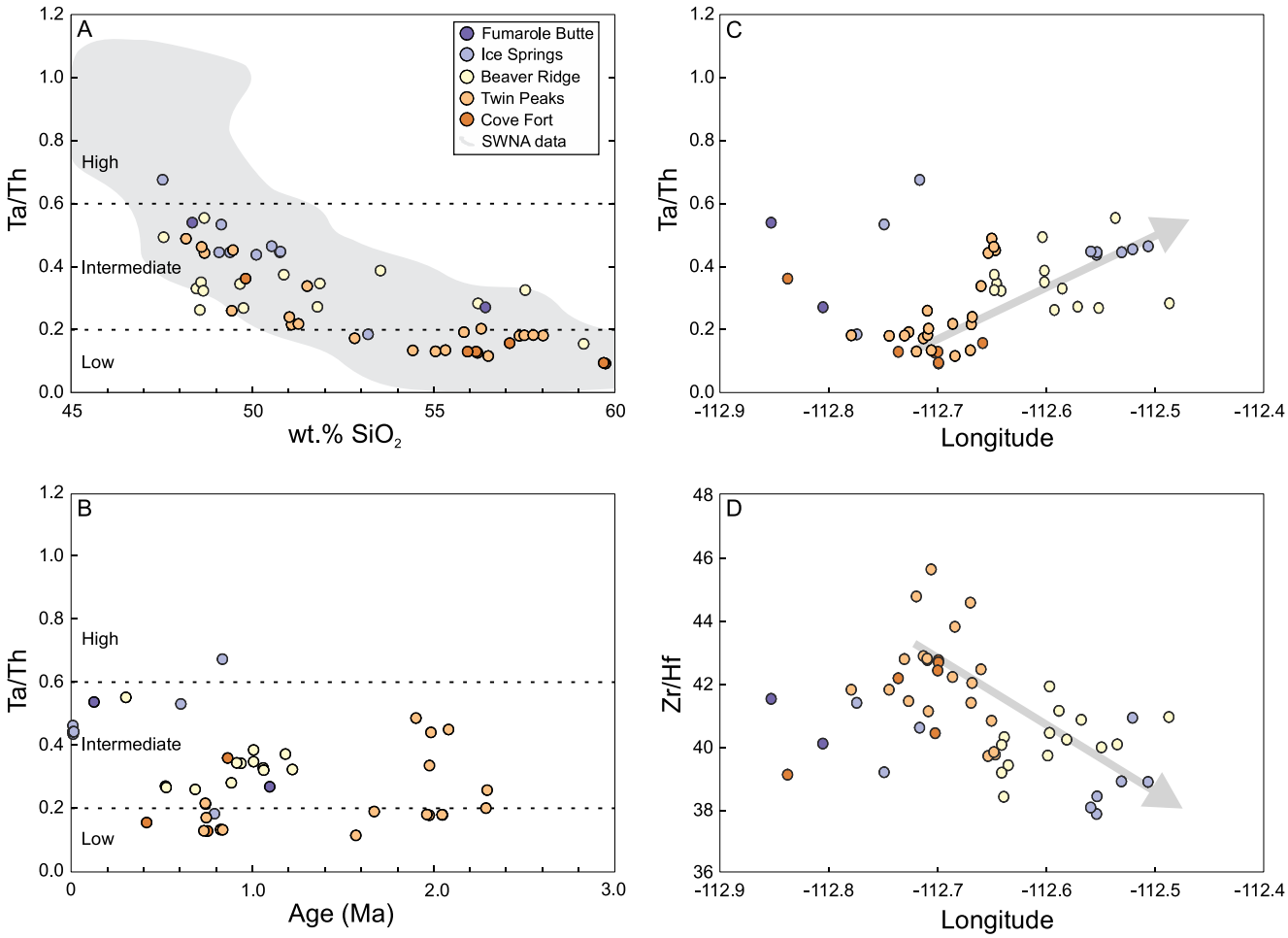

Figure 5. Trace element variation diagrams. (a) Ta/Th versus wt.% SiO_2 for BRD lavas. Most units have intermediate Ta/Th ratios. Southwest North America (SWNA) field from Farmer et al. (2020). (b) Ta/Th versus Age (Ma), which shows no strong temporal correlation. Ages are from this study and Rivera et al. (2024). (c) Ta/Th versus longitude. There is a general increase in Ta/Th toward the east of −112.7°, whereas (d) Zr/Hf decreases toward the east.

primary melt inclusions. Thus, trapped primary melt inclusions within K-poor phenocrysts such as olivine can enable $^{40}Ar/^{39}Ar$ geochronology of mafic rocks that may be otherwise unable to be dated with other techniques.

5.2. New Versus Published Ages From the BRD Volcanic Field

The new $^{40}Ar/^{39}Ar$ data are generally in agreement with previously published K-Ar and $^{40}Ar/^{39}Ar$ data from various BRD units (Best et al., 1980; Crecraft et al., 1981; Evans et al., 1980; Hoover, 1974; Johnsen et al., 2010, 2014; Nash, 1986) with several important exceptions. The K-Ar ages of Best et al. (1980) and Nash (1986) for the Cove Creek basalts to andesites from the Twin Peaks subfield range from 2.6 ± 0.4 to 2.2 ± 0.5 Ma, whereas our $^{40}Ar/^{39}Ar$ ages for this unit span 2.29 ± 0.06 Ma to as young as 1.67 ± 0.06 Ma (Table 1). Similarly, Beaver Ridge I andesite gave a K-Ar age of 1.5 ± 0.2 Ma (Nash, 1986) and a sample from the same locality gave a $^{40}Ar/^{39}Ar$ age of 1.18 ± 0.02 Ma (Table 1). The largest age discrepancy lies in the Burnt Mountain basalts and basaltic andesites from the Twin Peaks subfield, which have K-Ar ages of 2.1 ± 0.4 Ma and 2.2 ± 0.5 Ma (Nash, 1986), but $^{40}Ar/^{39}Ar$ ages of 0.837 ± 0.028 to 0.732 ± 0.014 Ma (Table 1). We suspect that the older K-Ar ages reflect inaccurate measurement of either the $^{40}Ar^*$ or K content of the extremely coarse whole-rock material melted for the K-Ar analyses more than four decades ago.

In addition to changing the ages of some of the BRD units, our new $^{40}Ar/^{39}Ar$ data also require a reevaluation of the timing of the eruptions of some BRD units relative to others. For example, ~100 kyrs elapsed between the eruption of the 2.44–2.41 Ma Twin Peaks rhyolites and the various mafic Cove Creek units of the Twin Peaks

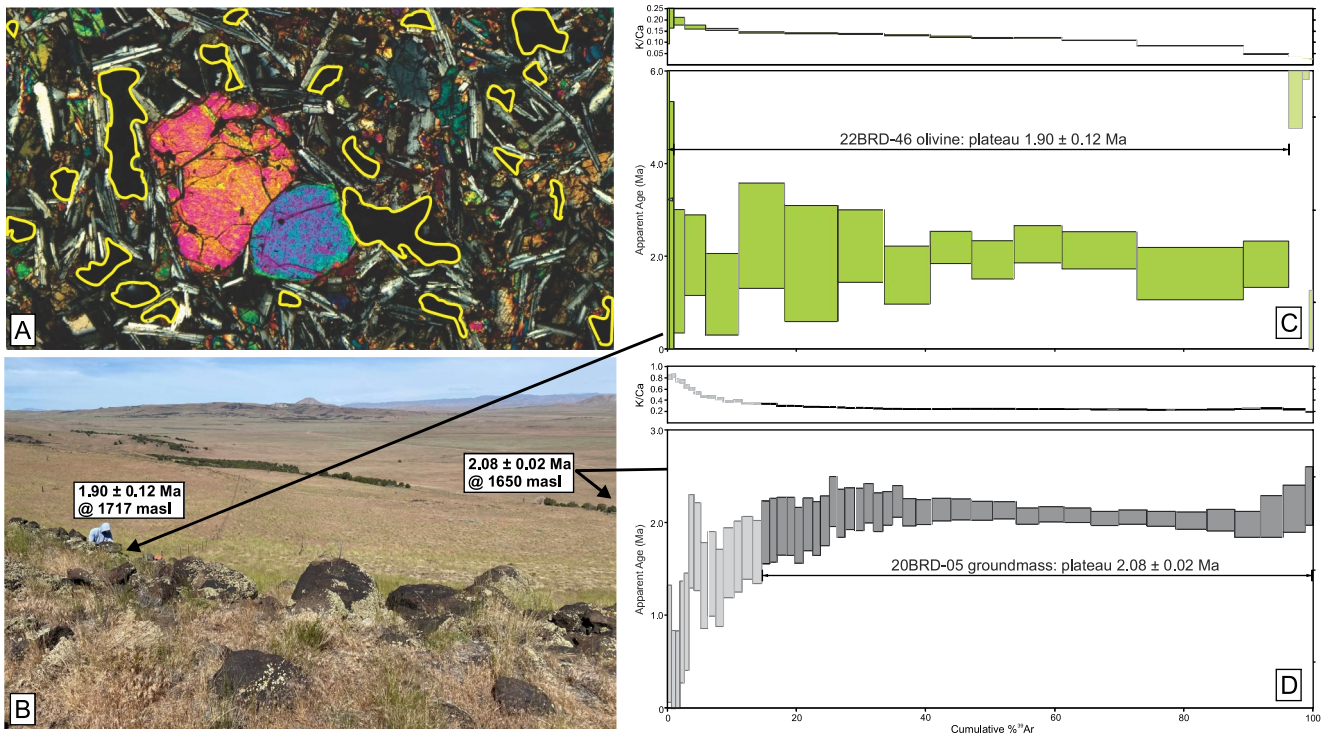

Figure 6. $^{40}Ar/^{39}Ar$ results from upper Cove Creek section, Twin Peaks subfield. (a) Image of thin section of 22BRD-46 showing the abundant vesicles present in the sample. (b) Photograph taken from atop ~70 m section of upper Cove Creek lavas showing the location of sample 22BRD-46 at 1717 m above sea level and approximate location of sample 20BRD-05 at 1650 m above sea level. (c) Age spectrum from olivine in 22BRD-46 with a plateau age of 1.90 ± 0.12 Ma. (d) Age spectrum from groundmass in 20BRD-05 with a plateau age of 2.08 ± 0.02 Ma.

subfield (2.30–1.67 Ma proto-Cove Creek, Cove Creek lower, Cove Creek upper), thereby refuting the suggestion of Johnsen et al. (2014) that the Twin Peaks rhyolites and basalts erupted simultaneously. Moreover, given that the Twin Peaks rhyolites preceded the basalts by ~100 kyrs, they are likely not genetically related to one another.

5.3. Migration of the BRD Volcanic Field and Local Tectonic Controls on Volcanism

Establishing the spatiotemporal eruptive patterns of Quaternary volcanic fields is key for identifying eruptive hazards (Zimmerer, 2024), constraining recurrence intervals (Valentine et al., 2021), understanding vent morphologies (Aguilera et al., 2022), and exploring controls on the origin of magmas and their associated vents (e.g., Rivera et al., 2024). Here we focus on the latter by evaluating the origin of BRD magmas and the migration pattern of BRD volcanism compared to other volcanic fields in the southwestern USA.

The mechanisms driving volcanic vent migration in the southwestern USA have been investigated for more than five decades (e.g., Christiansen & Lipman, 1972). While there is a consensus that vent location and migration are likely controlled by multiple factors (e.g., Connor et al., 1992), the relative role of each of the following major drivers continues to be debated: (a) North American plate motion, (b) asthenospheric convection and lithospheric erosion resulting in migration toward the center of the Colorado Plateau, (c) local and regional tectonic stress regimes, or (d) some combination of these processes.

For example, early work by Best and Hamblin (1978) and by Luedke and Smith (1978) used several K-Ar ages to suggest that volcanism in the southwestern USA migrated toward the Colorado Plateau. Numerous subsequent studies have also called upon progressive inward younging of Quaternary volcanism toward the center of the Colorado Plateau (e.g., Connor et al., 1992; Conway et al., 1997; Crow et al., 2011; Nelson & Tingey, 1997; Wenrich et al., 1995), including a recent assessment of seismic data in the southwestern US (Golos & Fischer, 2022).

In contrast, geochronologic and paleomagnetic data from the Springerville (Arizona), San Francisco (Arizona), and Raton-Clayton (New Mexico) volcanic fields suggest that volcanism has migrated eastward at ~2–3 cm/year

owing to the westward motion of the North American plate over a fixed lithospheric mantle source (Condit et al., 1989; Connor et al., 1992; Tanaka et al., 1986; Zimmerer, 2019). However, a recent in-depth study of the evolution of all the volcanic fields in New Mexico shed new light on the temporal changes in vent migration patterns (Zimmerer, 2024). Specifically, for volcanic fields with protracted histories that extend prior to the Quaternary Period, only the latest eruptions exhibit an eastward migration pattern. For example, volcanism in the Raton-Clayton field began at ca. 9.2 Ma, but the eastward migration began at 1.3 Ma. Similarly, volcanism in the Red Hill–Quemado area began at 8.0 Ma, but migration to the north–northeast initiated at ca. 2.5 Ma. Volcanic fields with shorter eruptive histories that are mostly confined to the Quaternary Period show vent migration to the east-northeast during their entire existence (Zimmerer, 2024). Thus, the transition from migration toward the Colorado Plateau to eastward migration occurs in the Quaternary, but the onset of this migration is variable. Zimmerer (2024) suggests that vent migration in the Quaternary is likely linked to North American plate motion over partial melt zones in the asthenospheric mantle, and the final location where magma reaches the Earth's surface is strongly influenced by structures in the uppermost crust.

Our new geochemical and geochronologic data can provide some clues as to the potential mechanisms that may be most important in controlling vent location and migration within the BRD volcanic field. In the Sevier Desert of central Utah, the origin of low-angle normal faulting, including that in the BRD volcanic field, continues to be contentious (e.g., DeCelles & Coogan, 2006). High-precision GPS velocities were used to constrain elastic dislocation models and to infer that dike injections into the uppermost crust are likely driving faulting in this region (Stahl & Niemi, 2017), and thus local extension is not controlling vent location and migration. In the central BRD, the oldest lavas at ∼2.45 Ma are located to the southwest and the youngest lavas from the Ice Springs subfield (660 years old) are located to the northeast (Figure 7). This trend would imply an average long-term migration rate of 1.4 cm/year over the last 2.45 Ma. It is only loosely consistent with the west-southwest motion of the North American plate in central Utah. However, this trend is parallel to the margin of the Colorado Plateau. In other words, it does not exactly follow a trend associated with North American Plate motion nor is it moving in toward the center of the plateau. Upon closer examination, the general northeasterly vent migration trend of the central BRD is not robust. The locus of volcanism moves from the Twin Peaks rhyolites at 2.4 Ma to almost due east to the Cove Creek basalts until 1.6 Ma. It then migrates to the north along Beaver Ridge at ∼1.0 Ma and then back to the south for the Burnt Mountain lavas until 0.73 Ma (Figure 7). The 0.884 Ma Kanosh scoria cones, which are located closest to the edge of the Colorado Plateau, are essentially at the same longitude as the youngest Ice Springs eruptions, which further invalidates a general northeasterly migration trend with time.

We attempt to use the BRD geochemical data to constrain the origins of the BRD magmas and their evolution over the last 2.5 million years, but there simply are not a lot of strong correlations amongst the various major and trace elements. Farmer et al. (2020) used Ta/Th values from Cenozoic volcanic rocks in the southwest US to demonstrate that the compositions of many mafic to intermediate lavas are controlled by rutile ± apatite-bearing sources. Rocks with intermediate Ta/Th ratios are inferred to have been sourced from metasomatized continental lithospheric mantle (CLM), which is deemed to be widespread (Farmer et al., 2020). Most BRD basalts and basaltic andesites have intermediate Ta/Th ratios (0.6–0.2; Figure 5a), which implies that they inherited some of their trace element composition from the existing CLM during ascent. Asthenosphere melting is required elsewhere in the Basin and Range where it generates high Ta/Th, OIB-like, sodic basalts (Farmer et al., 2024). In the BRD, the lack of high Ta/Th basalts does not preclude the presence of asthenospheric melts, but rather suggests that they have more extensively interacted with the CLM, probably while coalescing at the lithosphere-asthenosphere boundary (see Section 5.4 below). This suggestion is similar to that of Crow et al. (2011), who noted that alkali basalts in southern Utah and central Arizona show negative S and P wave anomalies but lack strong asthenospheric signatures. They suggest that these alkali basalts represent upwelling asthenosphere melts that have been modified by the lithosphere. The limited isotopic data available for the BRD (Johnsen et al., 2014) indicate that all mafic BRD lavas have ε_{Nd} values from −6 to −12, which likely requires extensive interaction with the lithosphere, some of which could be very low ε_{Nd} Archean lithosphere.

Ta/Th ratios generally increase to the east from −112.7° to −112.4° longitude, whereas Zr/Hf decreases over that same interval (Figures 5c and 5d). One interpretation could be that the easternmost lavas incorporated CLM with a slightly different composition. However, these geochemical trends with longitude more likely reflect differentiation as both Th and Zr are strongly correlated with wt.% SiO_2. It is worth noting that while basalts erupt everywhere in the BRD, evolved rocks (i.e., andesites through rhyolites) only erupt west of −112.6° longitude. The only exception to this trend is the 0.1 km^3 White Mountain rhyolite (Nash, 1986), which erupted at ∼−112.5°

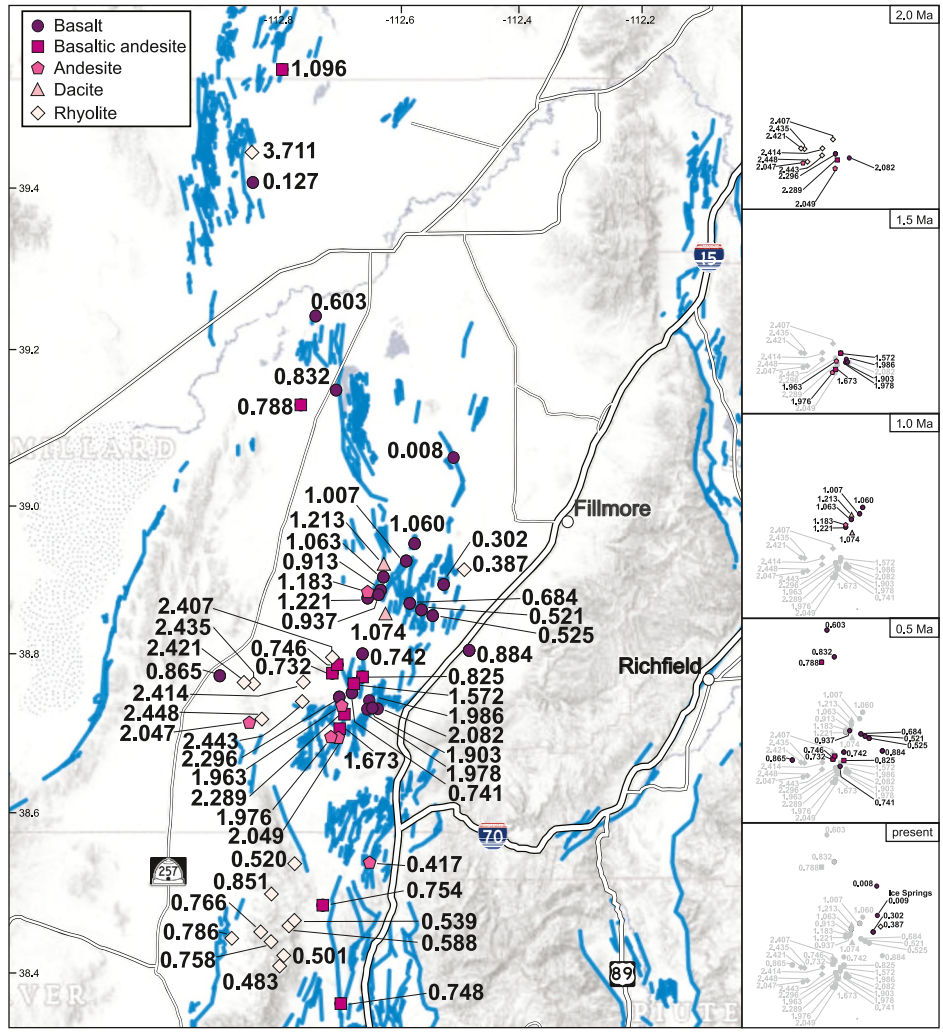

Figure 7. Locations and $^{40}Ar/^{39}Ar$ ages of BRD samples shown with a map of Quaternary faults in the Black Rock Desert from Ayling et al. (2022). Samples are colored based on erupted compositions. Panels on the right show eruptive history in intervals at 2.0, 1.5, 1.0, 0.5 Ma and what it looks like at present. Ice Springs age is from ^{36}Cl data of Judge et al. (2019).

(Figure 7). The origin of this compositional divide may be related to the composition and lithology of the crust beneath the western versus eastern BRD, a hypothesis that could be more thoroughly vetted with radiogenic isotope analyses (e.g., Rudzitis et al., 2016).

Most of the commonly evoked mechanisms for vent migration in the southwest US seem to not be applicable to the BRD, and thus another controlling factor must be at play. As noted by Zimmerer (2024) and numerous others, the role of local structures cannot be ignored as having an influence on vent location. In the BRD, almost all of the eruptions are coincident with Quaternary faults mapped by the Utah Geological Survey (Figure 7). A simple explanation is that the faults predate the eruptions and thus provide a pathway for magma ascent in the upper crust. Thus, the variable migration patterns within the BRD over the last 2.5 million years could simply be that magmas are opting for the easiest path to the surface following emplacement into the upper crust. However, Stahl and Niemi (2017) suggest that faulting in the BRD region is the result of dike injections associated with the Quaternary eruptions. Our new geochemical and geochronologic data have no bearing on this paradox. If Stahl and Niemi (2017) are indeed correct that the normal faults did not already exist and are not facilitating BRD lava emplacement, the random vent locations within the BRD may reflect a greater influence from deeper structures/sources within the lithosphere and asthenosphere.

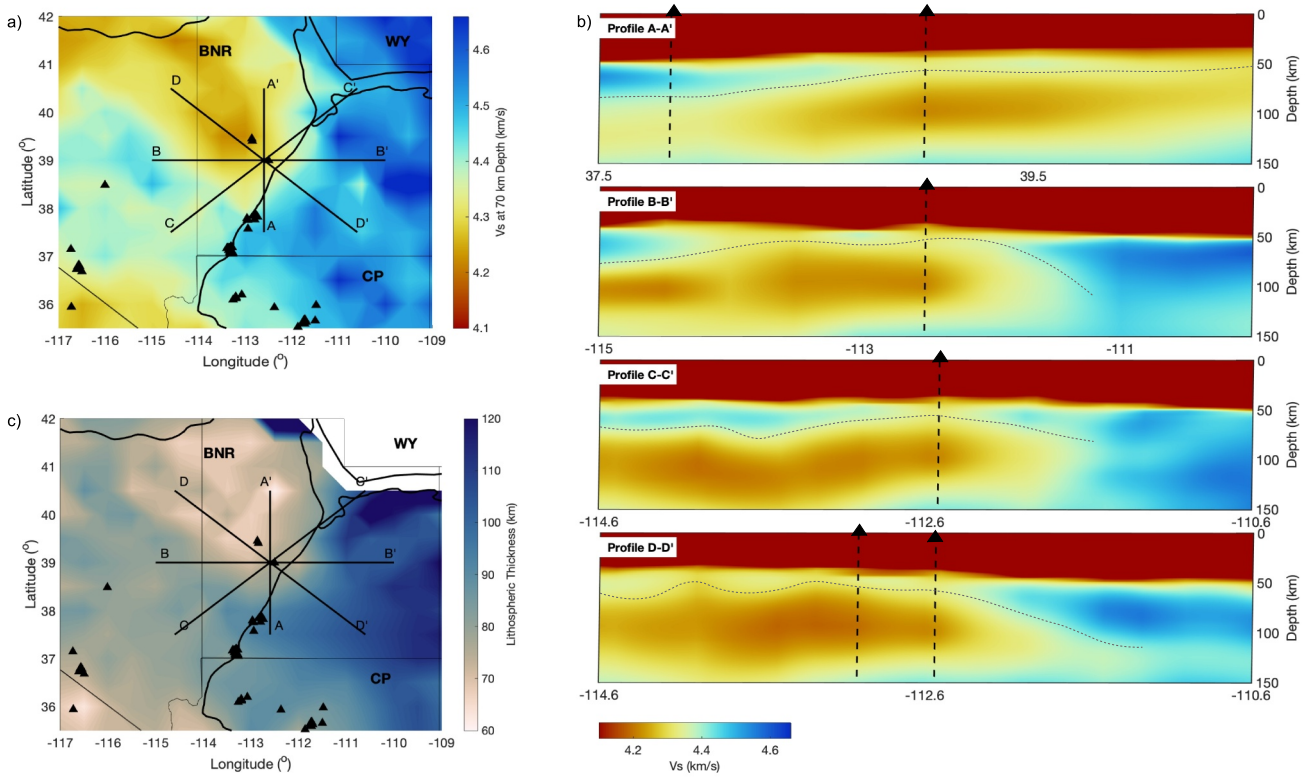

Figure 8. Shear wave velocity (Vs) within the lithosphere and asthenosphere below the Black Rock Desert volcanic field, from the model of Golos et al. (2024). (a) Vs at 70 km depth showing surface traces of cross-sections. Recent mafic volcanoes in the SW USA are shown in black triangles from the NAVDAT database (https://www.navdat.org/). Thick black lines indicate the boundaries of tectonic regions, from the USGS physiographic province map (https://data.usgs.gov/datacatalog/data/USGS:e04ea9e9-17b6-45ae-b279-7bc35ea79539): BNR—Basin and Range; WY—Wyoming Craton; CP—Colorado Plateau. (b) Cross-sections through the Vs model. Vertical black dashed lines indicate the locations of volcanoes from (a). All the cross-sections go through the Ice Springs subfield. Profile D-D′ intersects the Fumarole Butte subfield, which is also depicted with two black triangles in (a). Dashed gray lines indicate the approximate depth to base of lithosphere, indicating the lithosphere-asthenosphere boundary (LAB) where possible.

5.4. Deep Magmatic Processes Beneath the BRD Inferred From a Shear-Velocity Model

For a sense of the broader context in which these deeper structures/magma sources are situated, we examine several cross-sections through the shear-velocity (Vs) model presented by Golos et al. (2024). This model was determined through a Bayesian inversion of surface wave and converted body wave data for 1-D profiles of absolute Vs with depth, which are more sensitive to gradients in wavespeed (i.e., structures that relate to boundaries between the Earth's layers) compared to traditional body-wave or surface-wave tomography. The 1-D profiles may be assembled into a volume, from which a slice is interpolated, which displays vertical and lateral variations. Figure 8 shows several slices through this model below the BRD volcanic field. Furthermore, most Vs profiles in the southwestern US exhibit a decrease in Vs with increasing depth somewhere below the base of the crust. This decrease is interpreted as the Lithosphere-Asthenosphere Boundary (LAB), and the depth of the LAB is estimated to be the center of this decrease in Vs, as described in Golos et al. (2024). LAB depth is depicted in each vertical slice in Figure 8b, and in map-view in Figure 8c. We observe an anomalously thin lithosphere (<70 km) and low Vs (<4.2 km/s) below the BRD volcanic field, and a steep increase in lithospheric thickness and Vs to the east of the BRD.

The low values of Vs below the BRD are compatible with high temperature and partial melt. Below the Beaver Ridge site, the minimum mantle Vs of 4.17 km/s (with a standard deviation of 0.04 km/s) occurs at 92 km depth. This value corresponds to about a 7.1% decrease from the AK135 reference value at this depth (Kennett et al., 1995) (6.2% if Vs is one standard deviation above the reported value). Using the approximate relationship of a decrease of 2.1% in Vs per 100°C of Cammarano et al. (2003), this yields a temperature anomaly of 340°C (300°C for one standard deviation). Using a 1300°C potential temperature and gradient of 0.4˚C/km as a reference, the expected

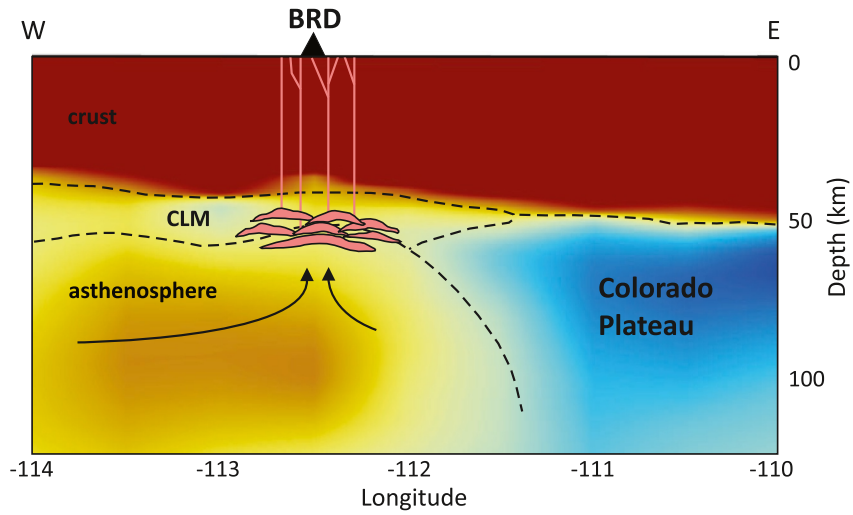

Figure 9. Schematic cross-section of asthenosphere-lithosphere system beneath the BRD volcanic field. Modified from Vs model in Figure 8. The concave downward dashed line represents the inferred lithosphere-asthenosphere boundary. Shear-driven upwelling due to mantle flow likely leads to (a) a thinned lithosphere and (b) asthenospheric melts coalescing at the base of the lithosphere and incorporating continental lithospheric mantle (CLM) as indicated by Ta/Th ratios (e.g., Farmer et al., 2020). Magmas subsequently ascend to the surface via a variety of pathways, resulting in a distributed volcanic field.

melt-free temperature at 92 km below the BRD is 1640°C (1600°C). Even considering that anelastic and premelting effects (e.g., Yamauchi & Takei, 2024) and the presence of melt itself (Hammond & Humphreys, 2000; Holtzman, 2016) would decrease the temperature contrast expected from the Vs anomaly, this temperature exceeds any realistic dry peridotite solidus (e.g., Hirschmann, 2000). Therefore, we conclude that it is difficult to achieve the geophysically inferred wavespeeds in the asthenosphere without invoking melting, but further modeling must be done to place quantitative constraints on the thermal state and melt fraction. Other more detailed inferences of melt fraction from seismic wavespeed modeling (e.g., Byrnes et al., 2023; Hier-Majumder & Tauzin, 2017; Porter & Reid, 2021), as well as magnetotelluric observations (Munch & Grayver, 2023), have also proposed that asthenospheric melt is present below the BRD. Similar inferences were made in the Milford Valley just west of the Mineral Mountains, where helium isotope data in concert with recently published geophysical data are attributed to mantle melts that ascended from the base of the crust (Simmons & Kirby, 2024).

It is possible that larger-scale mantle flow and its interactions with the LAB structure in the western Colorado Plateau are responsible for elevated temperatures and sub-lithospheric melting, and therefore play a role in BRD volcanism. The BRD contains the shallowest LAB in the region and is immediately adjacent to a step-like increase in lithospheric thickness at the edge of the Colorado Plateau. This lithospheric topography is thought to influence the patterns of mantle flow. Shear-wave splitting indicates an abrupt change in the direction of fast splitting at this transitional region (e.g., Lin et al., 2011; Zhou et al., 2018), becoming parallel to the edge of the Colorado Plateau. Furthermore, constraints from dynamic topography (Becker et al., 2014) and geodynamic modeling (e.g., Ballmer et al., 2015; van Wijk et al., 2010) suggest upward mantle flow at the edges of the Colorado Plateau (Figure 9). Such a flow pattern, especially in the context of elevated temperatures, would facilitate decompression melting below the BRD (Ballmer et al., 2015), and any mobile melt would naturally coalesce below the shallowest lithosphere.

Asthenospheric melt may itself be the ultimate source of volcanism in the BRD; thermobarometric modeling by Plank and Forsyth (2016) reported melt equilibration depths of 60 km, which coincides with the seismically inferred base of the lithosphere. It is also possible that the associated thermal anomaly may act to partially melt the lithosphere, particularly if it has been metasomatically altered, as suggested by Farmer et al. (2024). The chemical fingerprint of the continental lithospheric mantle (CLM) is pervasive within the BRD. However, unlike Farmer et al. (2024) who advocate for this signature to be the result of melt generation within the CLM, we suggest that asthenospheric melts pond at the base of the lithosphere and partially melt the CLM, thereby imparting its geochemical signature on the asthenospheric melts. Thus, the sublithospheric mantle below the BRD is an

important factor that sets the stage for a complicated interplay of mantle flow, tectonics, and pre-existing crustal and structural features.

6. Conclusions

We present 46 new $^{40}Ar/^{39}Ar$ ages ranging from 3.7 Ma to 8 ka for lavas, domes, and tephra within the Black Rock Desert (BRD) volcanic field in Utah. Included in this new data set are $^{40}Ar/^{39}Ar$ ages obtained on olivine from lavas that were too vesicular for $^{40}Ar/^{39}Ar$ geochronology, which represent a novel alternative approach for dating Quaternary mafic rocks that may not be datable with other techniques. The 46 BRD ages are combined with the 13 recently published $^{40}Ar/^{39}Ar$ ages from the Mineral Mountains to evaluate the spatiotemporal evolution of all five subfields of the BRD volcanic field. In the central BRD, the oldest lavas and domes are located in the southwest sector of the volcanic field and the youngest lavas, which are only a few hundred years old, are located ~30 km to the NNE. However, the vent migration patterns within the BRD over the last 2.5 Ma are non-uniform, and are not associated with North American Plate motion nor are they migrating inwards toward the center of the Colorado Plateau due to lithospheric erosion.

Trace element ratios such as Ta/Th suggest that BRD magmas are asthenospheric melts that have incorporated some metasomatized continental lithospheric mantle at the base of the lithosphere prior to ascent to the surface. Overall, the lithosphere-asthenosphere system in the southwest US is structurally complex. What process(es) (Basin and Range extension, local versus regional tectonics, erosion of the Colorado Plateau, etc.) are primarily controlling how BRD magmas go from the base of the lithosphere to the surface require interdisciplinary investigations to understand the relative contributions of each. Additional geodetic, geochemical (i.e., isotopic; e.g., Farmer et al., 2024), and seismic data in the BRD and southwestern US will undoubtedly improve our understanding of why volcanoes erupt where they do in distributed volcanic fields globally and will further illuminate the interplay between tectonics and volcanism.

Data Availability Statement

All data used in this study are presented in Table 1 and Supporting Information S1 and S2. Major element and trace element data and age determinations from the Mineral Mountains are from Rivera et al. (2024).

Acknowledgments
This project was supported by U.S. National Science Foundation Grants EAR-1940266 and EAR-1940305. Bryan Wathen is thanked for assistance with sample preparation. Emily Kleber at UGS is also thanked for numerous informative conversations about Quaternary faults in Utah. Constructive reviews by Lang Farmer, Kevin Konrad, and an anonymous reviewer helped improve the manuscript in many ways. The prompt editorial handling of Marie Edmonds is very much appreciated.

References

Aguilera, M., Ureta, G., Grosse, P., Németh, K., Aguilera, F., & Vilches, M. (2022). Geomorphological, morphometric, and spatial distribution analysis of the scoria cones in the Negros de Aras monogenetic volcanic field, northern Chile. *Journal of Volcanology and Geothermal Research*, *422*, 107458. https://doi.org/10.1016/j.jvolgeores.2021.107458

Armstrong, R. L., Ekren, E. B., McKee, E. H., & Noble, D. C. (1969). Space-time relations of Cenozoic silicic volcanism in the Great Basin of the western United States. *American Journal of Science*, *267*(4), 478–490. https://doi.org/10.2475/ajs.267.4.478

Ayling, B., Faulds, J., Morales Rivera, A., Koehler, R., Kreemer, C., Mlawsky, E., et al. (2022). INGENIOUS-Great Basin regional dataset compilation (No. 1391). *USDOE Geothermal Data Repository (United States); GBCGE, NBMG, UNR*.

Ballmer, M. D., Conrad, C. P., Smith, E. I., & Johnsen, R. (2015). Intraplate volcanism at the edges of the Colorado Plateau sustained by a combination of triggered edge-driven convection and shear-driven upwelling. *Geochemistry, Geophysics, Geosystems*, *16*(2), 366–379. https://doi.org/10.1002/2014GC005641

Becker, T. W., Faccenna, C., Humphreys, E. D., Lowry, A. R., & Miller, M. S. (2014). Static and dynamic support of western United States topography. *Earth and Planetary Science Letters*, *402*, 234–246. https://doi.org/10.1016/j.epsl.2013.10.012

Best, M. G., & Hamblin, W. K. (1978). Origin of the northern Basin and Range province; Implications from the geology of its eastern boundary. In R. B. Smith & G. P. Eaton (Eds.), *Cenozoic tectonics and regional geophysics of the western Cordillera* (Vol. 152, pp. 313–340). Geological Society of America.

Best, M. G., McKee, E. H., & Damon, P. E. (1980). Space-time-composition patterns of Late Cenozoic mafic volcanism, southwestern Utah and adjoining areas. *American Journal of Science*, *280*(10), 1035–1050. https://doi.org/10.2475/ajs.280.10.1035

Blackwell, D., Richards, M., Frone, Z., Ruzo, A., & Dingwall, R. (2011). Temperature-at-depth maps for the conterminous US and geothermal resource estimates: Geothermal Resources Council (GRC) Transactions (Vol. *35*, pp. 1545–1550).

Byrnes, J., Gaherty, J., & Hopper, E. (2023). Seismic architecture of the lithosphere-asthenosphere system in the western United States from a joint inversion of body- and surface-wave observations: Distribution of partial melt in the upper mantle. *Seismica*, *2*. https://doi.org/10.26443/seismica.v2i2.272

Cammarano, F., Goes, S., Vacher, P., & Giardini, D. (2003). Inferring upper-mantle temperatures from seismic velocities. *Physics of the Earth and Planetary Interiors*, *138*(3–4), 197–222. https://doi.org/10.1016/S0031-9201(03)00156-0

Christiansen, R. L., & Lipman, P. W. (1972). A discussion on volcanism and the structure of the Earth—Cenozoic volcanism and plate-tectonic evolution of the western United States. II. Late Cenozoic. *Philosophical Transactions of the Royal Society of London - A*, *271*(1213), 249–284.

Condit, C. D., Crumpler, L. S., Aubele, J. C., & Elston, W. E. (1989). Patterns of volcanism along the southern margin of the Colorado Plateau: The Springerville field. *Journal of Geophysical Research*, *94*(B6), 7975–7986. https://doi.org/10.1029/jb094ib06p07975

Connor, C. B., Condit, C. D., Crumpler, L. S., & Aubele, J. C. (1992). Evidence of regional structural controls on vent distribution: Springerville Volcanic Field, Arizona. *Journal of Geophysical Research*, *97*(B9), 12349–12359. https://doi.org/10.1029/92JB00929

Conrey, R. M., Bailey, D. G., Singer, J. W., Wagoner, L. J., Parfitt, B., Hay, J., et al. (2023). Combined use of multiple external and internal standards in LA-ICPMS analysis of bulk geological samples using lithium borate fused glass. *Geochemistry: Exploration, Environment, Analysis*, *23*(2), geochem2023-001. https://doi.org/10.1144/geochem2023-001

Conway, F. M., Ferrill, D. A., Hall, C. M., Morris, A. P., Stamatakos, J. A., Connor, C. B., et al. (1997). Timing of basaltic volcanism along the Mesa Butte Fault in the San Francisco volcanic field, Arizona from $^{40}Ar/^{39}Ar$ dates: Implications for longevity of cinder cone alignments. *Journal of Geophysical Research*, *102*(B1), 815–824. https://doi.org/10.1029/96JB02853

Crecraft, H. R., Nash, W. P., & Evans, S. H., Jr. (1981). Late Cenozoic volcanism at Twin Peaks, Utah—Geology and petrology. *Journal of Geophysical Research*, *86*(B11), 10303–10320. https://doi.org/10.1029/JB086iB11p10303

Crow, R., Karlstrom, K., Asmerom, Y., Schmandt, B., Polyak, V., & DuFrane, S. A. (2011). Shrinking of the Colorado Plateau via lithospheric mantle erosion: Evidence from Nd and Sr isotopes and geochronology of Neogene basalts. *Geology*, *39*(1), 27–30. https://doi.org/10.1130/G31611.1

DeCelles, P. G., & Coogan, J. C. (2006). Regional structure and kinematic history of the Sevier fold-and-thrust belt, central Utah. *Geological Society of America Bulletin*, *118*(7–8), 841–864. https://doi.org/10.1130/B25759.1

Evans, S. H., Jr., Crecraft, H. R., & Nash, W. P. (1980). K/Ar ages of silicic volcanism in the Twin Peaks/Cove Creek dome area. *Isochron/West*, *28*, 21–24.

Ewert, J. W., Diefenbach, A. K., & Ramsey, D. W. (2018). *2018 update to the U.S. Geological Survey national volcanic threat assessment* (p. 40). U.S. Geological Survey Scientific Investigations Report 2018–5140. https://doi.org/10.3133/sir20185140

Farmer, G. L., Fritz, D. E., & Glazner, A. F. (2020). Identifying metasomatized continental lithospheric mantle involvement in Cenozoic magmatism from Ta/Th values, southwestern North America. *Geochemistry, Geophysics, Geosystems*, *21*(5), e2019GC008499. https://doi.org/10.1029/2019GC008499

Farmer, G. L., Morgan, L., Cosca, M., Mize, J., Bailley, T., Turner, K., et al. (2024). Mantle melting in regions of thick continental lithosphere: Examples from Late Cretaceous and younger volcanic rocks, Southern Rocky Mountains, Colorado (USA). *Geosphere*, *20*(5), 1411–1440. https://doi.org/10.1130/GES02749.1

Galyardt, G. L., & Rush, F. E. (1981). *Geologic map of the Crater Springs known geothermal resources area and vicinity, Juab and Millard Counties, Utah (No. USGS/MAP/I-1297)*. US Geological Survey.

Golos, E. M., Brunsvik, B., Eilon, Z., Fischer, K. M., Byrnes, J., & Gaherty, J. (2024). A new view of shear wavespeed and the lithosphere-asthenosphere boundary in the Southwestern United States. *Journal of Geophysical Research: Solid Earth*, *129*(8), e2024JB029220. https://doi.org/10.1029/2024JB029220

Golos, E. M., & Fischer, K. M. (2022). New insights into lithospheric structure and melting beneath the Colorado Plateau. *Geochemistry, Geophysics, Geosystems*, *23*(3), e2021GC010252. https://doi.org/10.1029/2021GC010252

Gómez-Vasconcelos, M. G., Macías, J. L., Avellán, D. R., Sosa-Ceballos, G., Garduño-Monroy, V. H., & Cisneros-Máximo, G. (2020). The control of preexisting faults on the distribution, morphology, and volume of monogenetic volcanism in the Michoacán-Guanajuato Volcanic Field. *Bulletin of the Geological Society of America*, *132*(11–12), 2455–2474.

Hammond, W. C., & Humphreys, E. D. (2000). Upper mantle seismic wave velocity: Effects of realistic partial melt geometries. *Journal of Geophysical Research*, *105*(B5), 10975–10986. https://doi.org/10.1029/2000JB900041

Hier-Majumder, S., & Tauzin, B. (2017). Pervasive upper mantle melting beneath the western US. *Earth and Planetary Science Letters*, *463*, 25–35. https://doi.org/10.1016/j.epsl.2016.12.041

Hintze, L. F., Willis, G. C., Laes, D. Y., Sprinkel, D. A., & Brown, K. D. (2000). *Digital geologic map of Utah*. Utah Geological Survey.

Hirschmann, M. M. (2000). Mantle solidus: Experimental constraints and the effects of peridotite composition. *Geochemistry, Geophysics, Geosystems*, *1*(10), 1042. https://doi.org/10.1029/2000GC000070

Holtzman, B. K. (2016). Questions on the existence, persistence, and mechanical effects of a very small melt fraction in the asthenosphere. *Geochemistry, Geophysics, Geosystems*, *17*(2), 470–484. https://doi.org/10.1002/2015GC006102

Hoover, J. D. (1974). Periodic Quaternary volcanism in the Black Rock Desert, Utah. In J. K. Rigby (Ed.), *Brigham Young Univ. Geol. Stud* (Vol. 21, pp. 3–72).

Hopper, E., & Fischer, K. M. (2018). The changing face of the lithosphere-asthenosphere boundary: Imaging continental scale patterns in upper mantle structure across the contiguous U.S. with Sp converted waves. *Geochemistry, Geophysics, Geosystems*, *19*(8), 2593–2614. https://doi.org/10.1029/2018GC007476

Jicha, B. R., Schaen, A. J., Wathen, B. A., & Nachlas, W. O. (2024). Precambrian to Pleistocene $^{40}Ar/^{39}Ar$ dating of clinopyroxene-hosted melt inclusions. *Geology*, *52*(4), 287–291. https://doi.org/10.1130/G51777.1

Jicha, B. R., Singer, B. S., & Sobol, P. (2016). Re-evaluation of the ages of $^{40}Ar/^{39}Ar$ sanidine standards and supereruptions in the western U.S. using a Noblesse multi-collector mass spectrometer. *Chemical Geology*, *431*, 54–66. https://doi.org/10.1016/j.chemgeo.2016.03.024

Johnsen, R., Smith, E. I., & Walker, J. D. (2014). The 2.7–2.1 Ma Twin Peaks caldera—Stratigraphy and petrogenesis. In J. S. MacLean, R. F. Biek, & J. E. Huntoon (Eds.), *Geology of Utah's Far South* (Vol. 43, pp. 617–638). Association of Public.

Johnsen, R. L., Smith, E. I., & Biek, R. F. (2010). Subalkaline volcanism in the black Rock Desert and Markagunt Plateau volcanic fields of south-central Utah. *Utah Geological Association Publication*, *39*, 101–150.

Judge, S., Pollock, M., Williams, M., Schantz, K., Baxstrom, K., Burden, K., et al. (2019). *Young volcanism in Millard County, Utah Geol* (Vol. 1, pp. 1–13). Association of Public.

Kennett, B. L. N., Engdahl, E. R., & Buland, R. (1995). Constraints on seismic velocities in the Earth from travel times. *Geophysical Journal International*, *122*(1), 108–124. https://doi.org/10.1111/j.1365-246x.1995.tb03540.x

King, S. D., & Anderson, D. L. (1998). Edge-driven convection. *Earth and Planetary Science Letters*, *160*(3), 289–296. https://doi.org/10.1016/S0012-821X(98)00089-2

Kuiper, K., Deino, A., Hilgen, F., Krijgsman, W., Renne, P., & Wijbrans, J. (2008). Synchronizing rock clocks of Earth history. *Science*, *320*(5875), 500–504. https://doi.org/10.1126/science.1154339

LeBas, M. J., Le Maitre, R. W., Streckeisen, A., & Zanettin, B. (1986). A chemical classification of volcanic rocks based on the total alkali silica diagram. *Journal of Petrology*, *27*(3), 745–750. https://doi.org/10.1093/petrology/27.3.745

Lee, J. Y., Marti, K., Severinghaus, J. P., Kawamura, K., Yoo, H. S., Lee, J. B., & Kim, J. S. (2006). A redetermination of the isotopic abundances of atmospheric Ar. *Geochimica et Cosmochimica Acta*, *70*(17), 4507–4512.

Leonard, G. S., Calvert, A. T., Hopkins, J. L., Wilson, C. J., Smid, E. R., Lindsay, J. M., & Champion, D. E. (2017). High-precision 40Ar/39Ar dating of Quaternary basalts from Auckland Volcanic Field, New Zealand, with implications for eruption rates and paleomagnetic correlations. *Journal of Volcanology and Geothermal Research*, *343*, 60–74. https://doi.org/10.1016/j.jvolgeores.2017.05.033

Lin, F. C., Ritzwoller, M., Yang, Y., Moschetti, M. P., & Fouch, M. J. (2011). Complex and variable crustal and uppermost mantle seismic anisotropy in the western United States. *Nature Geoscience*, *4*(1), 55–61. https://doi.org/10.1038/ngeo1036

Liu, K., Levander, A., Niu, F., & Miller, M. S. (2011). Imaging crustal and upper mantle structure beneath the Colorado Plateau using finite frequency Rayleigh wave tomography. *Geochemistry, Geophysics, Geosystems*, *12*(7), Q07001. https://doi.org/10.1029/2011GC003611

Luedke, R. G., & Smith, R. L. (1978). Map showing distribution, composition, and age of the late Cenozoic volcanic centers in Arizona and New Mexico. In *U.S. Geological Survey of Miscellaneous Investigations Series maps I-1091-A, scale 1:1,000,000*.

McDougall, I., Polach, H. A., & Stipp, J. J. (1969). Excess radiogenic argon in young subaerial basalts from the Auckland volcanic field, New Zealand. *Geochimica et Cosmochimica Acta*, *33*(12), 1485–1520. https://doi.org/10.1016/0016-7037(69)90152-5

Min, K., Mundil, R., Renne, P. R., & Ludwig, K. R. (2000). A test for systematic errors in $^{40}Ar/^{39}Ar$ geochronology through comparison with U/Pb analysis of a 1.1-Ga rhyolite. *Geochimica et Cosmochimica Acta*, *64*(1), 73–98. https://doi.org/10.1016/S0016-7037(99)002045

Mixon, E. E., Jicha, B. R., Tootell, D., & Singer, B. S. (2022). Optimizing $^{40}Ar/^{39}Ar$ analyses using an Isotopx NGX-600 mass spectrometer. *Chemical Geology*, *593*, 120753. https://doi.org/10.1016/j.chemgeo.2022.120753

Munch, F. D., & Grayver, A. (2023). Multi-scale imaging of 3-D electrical conductivity structure under the contiguous US constrains lateral variations in the upper mantle water content. *Earth and Planetary Science Letters*, *602*, 117939. https://doi.org/10.1016/j.epsl.2022.117939

Nash, W. P. (1986). *Distribution, lithology and ages of Late Cenozoic volcanism on the eastern margin of the Great Basin, west-central Utah* (p. 82). Final report to the Department of Energy, Contract DEAC0780.

Nelson, S. T., & Tingey, D. G. (1997). Time-transgressive and extension-related basaltic volcanism in southwest Utah and vicinity. *GSA Bulletin*, *109*(10), 1249–1265. https://doi.org/10.1130/0016-7606(1997)109<1249:TTAERB>2.3.CO;2

Oviatt, C. G. (1991). Quaternary geology of the Black Rock Desert, Millard County, Utah (No. 73). *Utah Geological Survey*. https://doi.org/10.34191/ofr-128

Oviatt, C. G. (2015). Chronology of Lake Bonneville, 30,000 to 10,000 yr BP. *Quaternary Science Reviews*, *110*, 166–171. https://doi.org/10.1016/j.quascirev.2014.12.016

Oviatt, C. G., & Nash, W. P. (1989). Late Pleistocene basaltic ash and volcanic eruptions in the Bonneville basin, Utah. *Geological Society of America Bulletin*, *101*(2), 292–303. https://doi.org/10.1130/0016-7606(1989)101<0292:lpbaav>2.3.co;2

Plank, T., & Forsyth, D. W. (2016). Thermal structure and melting conditions in the mantle beneath the Basin and Range province from seismology and petrology. *Geochemistry, Geophysics, Geosystems*, *17*(4), 1312–1338. https://doi.org/10.1002/2015GC006205

Porter, R., & Reid, M. (2021). Mapping the thermal lithosphere and melting across the continental US. *Geophysical Research Letters*, *48*(7), e2020GL092197. https://doi.org/10.1029/2020GL092197

Preece, K., Mark, D. F., Barclay, J., Cohen, B. E., Chamberlain, K. J., Jowitt, C., et al. (2018). Bridging the gap: $^{40}Ar/^{39}Ar$ dating of volcanic eruptions from the 'age of Discovery. *Geology*, *46*(12), 1035–1038. https://doi.org/10.1130/G45415.1

Rivera, T. A., Jicha, B. R., Kirby, S., & Peacock, H. B. (2024). Temporal, spatial, and chemical evolution of Quaternary high-silica rhyolites in the Mineral Mountains, Utah (No. 1890-K). *US Geological Survey*.

Rudzitis, S., Reid, M. R., & Blichert-Toft, J. (2016). On edge melting under the Colorado Plateau margin. *Geochemistry, Geophysics, Geosystems*, *17*(7), 2835–2854. https://doi.org/10.1002/2016gc006349

Schaen, A. J., Jicha, B. R., Hodges, K. V., Vermeesch, P., Stelten, M. E., Mercer, C. M., et al. (2021). Interpreting and reporting $^{40}Ar/^{39}Ar$ geochronologic data. *Geological Society of America Bulletin*, *133*(3–4), 461–487. https://doi.org/10.1130/B35560.1

Shen, W., Ritzwoller, M. H., & Schulte-Pelkum, V. (2013). A 3-D model of the crust and uppermost mantle beneath the Central and Western US by joint inversion of receiver functions and surface wave dispersion. *Journal of Geophysical Research: Solid Earth*, *118*, 262–276. https://doi.org/10.1029/2012JB009602

Simmons, S. F., & Kirby, S. (2024). Formation of a large cold groundwater mantle helium anomaly and high temperature geothermal resources in response to bimodal magmatism near Roosevelt Hot Springs and Utah FORGE, Milford Valley, southwest Utah. *Geochemistry, Geophysics, Geosystems*, *25*(9), e2024GC011539. https://doi.org/10.1029/2024GC011539

Stahl, T., & Niemi, N. A. (2017). Late quaternary faulting in the Sevier Desert driven by magmatism. *Scientific Reports*, *7*(1), 44372. https://doi.org/10.1038/srep44372

Tanaka, K. L., Shoemaker, E. M., Ulrich, G. E., & Wolfe, E. W. (1986). Migration of volcanism in the San Francisco volcanic field, Arizona. *Geological Society of America Bulletin*, *97*(2), 129–141. https://doi.org/10.1130/0016-7606(1986)97<129:MOVITS>2.0.CO;2

Valastro, S., Jr., Davis, E. M., & Varela, A. G. (1972). University of Texas at Austin radiocarbon dates IX. *Radiocarbon*, *14*(2), 461–485. https://doi.org/10.1017/s0033822200059506

Valentine, G. A., Ort, M. H., & Cortés, J. A. (2021). Quaternary basaltic volcanic fields of the American Southwest. *Geosphere*, *17*(6), 2144–2171. https://doi.org/10.1130/GES02405.1

van Wijk, J. W., Baldridge, W. S., van Hunen, J., Goes, S., Aster, R., Coblentz, D. D., et al. (2010). Small-scale convection at the edge of the Colorado Plateau: Implications for topography, magmatism, and evolution of Proterozoic lithosphere. *Geology*, *38*(7), 611–614. https://doi.org/10.1130/G31031.1

Von Tish, D. B., Allmendinger, R. W., & Sharp, J. W. (1985). History of Cenozoic extension in central Sevier Desert, west-central Utah, from COCORP seismic reflection data. *AAPG Bulletin*, *69*, 1077–1087. https://doi.org/10.1306/ad462b7d-16f7-11d7-8645000102c1865d

Wallace, P. J., Plank, T., Bodnar, R. J., Gaetani, G. A., & Shea, T. (2021). Olivine-hosted melt inclusions: A microscopic perspective on a complex magmatic world. *Annual Review of Earth and Planetary Sciences*, *49*(1), 465–494. https://doi.org/10.1146/annurev-earth-082420-060506

Wenrich, K. J., Billingsley, G. H., & Blackerby, B. A. (1995). Spatial migration and compositional changes of Miocene-Quaternary magmatism in the western Grand Canyon. *Journal of Geophysical Research*, *100*(B6), 10417–10440. https://doi.org/10.1029/95JB00373

Yamauchi, H., & Takei, Y. (2024). Effect of melt on polycrystal anelasticity. *Journal of Geophysical Research: Solid Earth*, *129*(4), e2023JB027738. https://doi.org/10.1029/2023JB027738

Zhou, Q., Liu, L., & Hu, J. (2018). Western US volcanism due to intruding oceanic mantle driven by ancient Farallon slabs. *Nature Geoscience*, *11*(1), 70–76. https://doi.org/10.1038/s41561-017-0035-y

Zimmerer, M. J. (2019). $^{40}Ar/^{39}Ar$ geochronology, vent migration patterns, and hazard implications of the youngest eruptions in the Raton-Clayton volcanic field. *New Mexico Geological Society Guidebook*, *70*, 151–160.

Zimmerer, M. J. (2024). A temporal dissection of late Quaternary volcanism and related hazards within the Rio Grande rift and along the Jemez lineament of New Mexico, USA. *Geosphere*, *20*(2), 505–546. https://doi.org/10.1130/GES02576.1